Convective Heat Transfer in Rotating, Circular Channels

by

Brenna Elizabeth Hogan

Submitted to the
Department of Mechanical Engineering
in Partial Fulfillment of the Requirements for the Degree of

Bachelor of Science in Engineering as Recommended by the
Department of Mechanical Engineering

at the

Massachusetts Institute of Technology

June 2012

Signature of Author: _____
Department of Mechanical Engineering
May 25, 2012

Certified by: _____
Cullen R. Buie
Mitsui Career Development Assistant Professor
Thesis Supervisor

Accepted by: _____
John H. Lienhard V
Samuel C. Collins Professor of Mechanical Engineering
Undergraduate Officer

Convective Heat Transfer in Rotating, Circular Tubes

by

Brenna Elizabeth Hogan

Submitted to the Department of Mechanical Engineering
on May 25, 2012 in Partial Fulfillment of the
Requirements for the Degree of

Bachelor of Science in Engineering as Recommended by the
Department of Mechanical Engineering

ABSTRACT

Nusselt number values for flow in a rotating reference frame are obtained through computational fluid dynamic (CFD) analysis for Rossby numbers Ro ~1-4 and Reynolds numbers Re ~1,000-2,000. The heat-transfer model is first validated according to Nusselt number correlations for laminar, developing flow in circular tubes and by friction factor correlations for fully developed flow in circular tubes rotating at constant angular velocity about an orthogonal axis. The data show heat-transfer enhancement for increasing rotational speeds, as predicted through secondary flows caused by Coriolis forces. Moreover, the heat-transfer enhancement is found to be greater than the resulting increase in friction losses due to secondary flows.

Thesis Supervisor: Cullen R. Buie
Tile: Mitsui Career Development Assistant Professor

Acknowledgements

I would like to thank my thesis supervisor, Professor Cullen R. Buie, for his guidance and patience.

I am indebted to Dr. Lino Gonzalez for his help, support, and patience throughout the process. I am grateful for all the time he devoted to helping me, and I have learned so much from him.

I would like to thank my friends and family who supported me throughout the many trials of MIT.

Last but certainly not least, I would like to thank my parents- I couldn't have asked for better.

Table of Contents

List of Figures

List of Tables

List of Variables

v = mean axial velocity

Ω_0 = constant angular velocity

D = diameter of pipe

μ = dynamic viscosity

ρ = density

ϑ = kinematic viscosity

L = axial length of channel

k = thermal conductivity

c_p = specific heat

z = axial location

ε = viscous dissipation

q = heat generation in the fluid (i.e. from a chemical reaction)

h = coefficient of convective heat transfer

$\bar{V}$ = velocity vector in inertial frame

$\overline{V^*}$ = velocity vector in rotating reference frame

$\bar{\Omega}$ = angular velocity vector

$\bar{F}$ = vector of body forces in the stationary reference frame (i.e. gravity)

$\bar{r}$ = radial position vector

P = static pressure

P^* = dynamic pressure in rotating system

T_s = wall surface temperature

Q_{conv} = total heat transfer rate to the fluid through convection

$\bar{h}$ = average heat transfer coefficient

A_s = tube surface area, πDL

ΔT_{lm}= log-mean temperature difference

T_{mo} = mean outlet temperature

T_{mi} = mean inlet temperature

$\Delta T_o \equiv T_s - T_{mo}$

$\Delta T_i \equiv T_s - T_{mi}$

$\dot{m}$ = mass flow rate

1. Introduction

The study of flow and heat transfer in the rotating reference frame has important implications for real world applications. Rotation gives rise to secondary flows, perpendicular to the primary radial flow. These secondary flows are produced by Coriolis forces in the rotating reference frame. The case of a straight circular cross-section channel rotating around a perpendicular axis, as shown in Figure 1, is examined in this work.

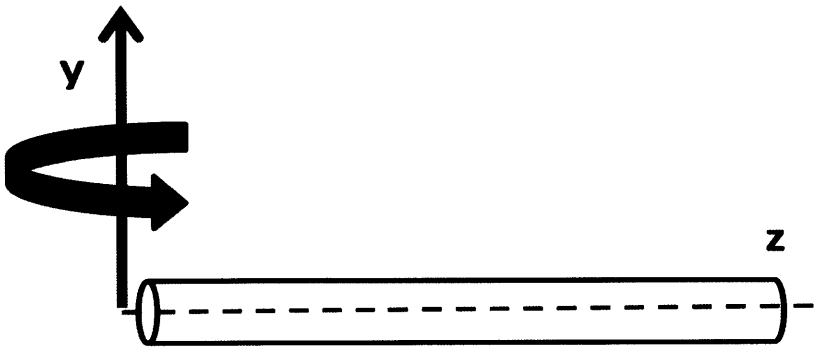

Figure 1. Circular cross-section tube rotating about perpendicular axis

Rotation is relevant in the study of cooling passages because rotation influences cooling performance via secondary flows generated because of Coriolis forces and centripetal buoyancy [6]. Rotation improves heat transfer from the stationary case by increasing heat transfer on the trailing edge of the channel compared to the leading edge, resulting in an overall increase in the convective heat transfer coefficient. However, an increase in the flow resistance from the stationary case is also seen with rotation. A study of the influence of rotation of various geometries on heat transfer and flow resistance has practical importance in the development of cooling technologies, such as in rotating cooling passages used in cooling systems for the rotor blades of gas turbines.

The objective of this work is to study heat transfer in rotating tubes of circular cross-section and to obtain Nusselt number and friction factor correlations for various flow conditions. In this work, we consider developing laminar flow at constant wall temperature subject to perpendicular rotation, where the flow direction is perpendicular to the axis of rotation. In particular, the focus is on the limiting case where the flow is purely radial, as depicted in Figure 1.

2. Formulation of the Problem

We consider the motion of a fluid in a channel rotating with a constant angular velocity. The Navier Stokes, or momentum, equation in the inertial reference frame is given by:

$$\rho\left(\frac{D\bar{V}}{Dt}\right) = \nabla P + \mu\nabla^2\bar{V} + \bar{F} \tag{1}$$

where the left hand side describes acceleration of the fluid particle and the right hand side is a summation of body forces and divergence of stress including pressure and shear stress. In the rotating frame of reference, the total derivative term of the left-hand side becomes

$$\frac{D\bar{V}}{Dt} = \frac{\partial \overline{V^*}}{\partial t} + \overline{V^*} \cdot \nabla \overline{V^*} + \bar{\Omega} \times (\bar{\Omega} \times \bar{r}) + 2\bar{\Omega} \times \overline{V^*} \tag{2}$$

where $\bar{\Omega} \times (\bar{\Omega} \times \bar{r})$ is the centrifugal force and $2\bar{\Omega} \times \overline{V^*}$ is the Coriolis force. Substituting the rotational terms to the Navier-Stokes gives

$$\frac{\partial \overline{V^*}}{\partial t} + \overline{V^*} \cdot \nabla \overline{V^*} = \frac{-\nabla \mathrm{P}}{\rho} - \bar{\Omega} \times (\bar{\Omega} \times \bar{r}) + \vartheta \nabla^2 \overline{V^*} - 2[\bar{\Omega} \times \overline{V^*}] + \bar{F} \tag{3}$$

By vector identity, the centrifugal acceleration term can be expressed as

$$-\bar{\Omega} \times (\bar{\Omega} \times \bar{r}) = \frac{1}{2} \nabla(|\bar{\Omega} \times \bar{r}^2|) \tag{4}$$

A new pressure-like variable P^* can be defined as

$$P^* = P - \frac{1}{2}|\bar{\Omega} \times \bar{r}\,|^2 \tag{5}$$

which represents the pressure modified by the centrifugal force [1]. This substitution is commonly made in the rotating reference frame to separate dynamic from hydrostatic pressure. Since the flow is steady with respect to the rotating coordinate system and gravitational forces are assumed to be negligible, the time derivative term on the left hand side of Equation (3) disappears and the vector of body forces in the stationary reference frame, $\bar{F}$, on the right hand side disappears as well. Equation (3) thus becomes

$$\overline{V^*} \cdot \nabla \overline{V^*} = \frac{-\nabla P^*}{\rho} + \vartheta \nabla^2 \overline{V^*} - 2[\bar{\Omega} \times \overline{V^*}] \tag{6}$$

Equation (6) can be non-dimensionalized by introducing the dimensionless variables

$$\overline{V^*}' = \frac{\overline{V^*}}{v}, \qquad \left(\frac{P^*}{\rho}\right)' = \left(\frac{P^*}{\rho}\right)\frac{1}{v^2}, \qquad \bar{\Omega}' = \frac{\bar{\Omega}}{\Omega_o}, \qquad \nabla' = \mathrm{D}\nabla$$

which gives

$$\overline{V^*}' \cdot \nabla' \overline{V^*}' = \frac{-\nabla' P^{*'}}{\rho} + \frac{\vartheta}{Dv} \nabla'^2 \overline{V^*}' - \frac{2\mathrm{D}\Omega_o}{\mathrm{v}} [\bar{\Omega}' \times \overline{\mathrm{V}^*}'] \tag{7}$$

The inverse Reynold and Rossby numbers appear from the dimensionless momentum equation. Substituting the known dimensionless parameters, we obtain

$$\overline{V^*}' \cdot \nabla' \overline{V^*}' = \frac{-\nabla' P^{*'}}{\rho} + \frac{1}{Re} \nabla'^2 \overline{V^*}' - \frac{1}{\mathrm{Ro}} [\bar{\Omega}' \times \overline{\mathrm{V}^*}'] \tag{8}$$

The non-dimensional Reynolds and Rossby numbers are explicitly given as

$$Re = \frac{Dv}{\vartheta} \tag{9}$$

$$\mathrm{Ro} = \frac{\mathrm{v}}{2\mathrm{D}\Omega_0} \tag{10}$$

The Reynolds number is a dimensionless number that is the ratio of inertial to viscous forces. Laminar flow occurs at low Reynold's numbers where viscous forces dominate the flow and the flow is characteristically smooth. At high Reynold's numbers, the flow is dominated by inertial forces which tend to produce eddies, vortices, and other flow instabilities, and the flow is said to be turbulent. The Rossby number is the ratio of inertial to Coriolis forces. A small Rossby number signifies flow strongly affected by Coriolis forces, and a large Rossby number indicates flow in which inertial and centrifugal forces dominate.

In addition to the momentum equation, the continuity equation given by

$$\frac{\partial \rho}{\partial t} + \nabla \rho \overline{V^*} = 0 \tag{11}$$

and the energy equation is

$$\rho c_p \left(\frac{\partial T}{\partial t} + \overline{V^*} \nabla T\right) = \nabla(k \nabla T) + \rho(\varepsilon + q) \tag{12}$$

where ε represents viscous dissipation in the fluid and q represents heat generation in the fluid (i.e. from a chemical reaction), and k is the thermal conductivity of the fluid. Our flow is steady, includes no viscous dissipation or chemical reactions, and we assume constant properties. For our flow, the energy equation then becomes

$$\bar{V} \nabla T = \alpha \nabla^2 T \tag{13}$$

Where $\alpha = \frac{k}{\rho c_p}$ is the thermal diffusivity of the fluid. The choice of non-dimensionalizing parameters in this case will be D, α, and v.

$$\frac{Dv}{\alpha} \bar{V} \nabla T = \alpha \nabla^2 T \tag{14}$$

The dimensionless group on the left-hand side is defined as the Peclet number,

$$Pe = \frac{Dv}{\alpha} = RePr \tag{15}$$

where

$$Pr = \frac{\vartheta}{\alpha} \tag{16}$$

The Prantl number is a dimensionless number which is the ratio of momentum diffusivity to thermal diffusivity. Our experiments involve air, which has a Prandtl number of 0.7. With a Prandtl number ~ 1, the momentum and thermal boundary layers will develop at the approximately the same rate, so the hydrodynamic and thermal entrance lengths are approximately equal.

Based on the dimensionless analysis just performed, we expect the heat-transfer coefficient in a fully developed rotating system to be a function of the three dimensionless parameters: *Re, Ro, Pr.* In the case of developing flow, we therefore expect the Nusselt number Nu to be governed by the relationship

$$Nu = f\left(Re, Ro, Pr, \frac{L}{D}\right) \tag{17}$$

This analysis supplemented in the following section by dimensional analysis using the Buckingham-Pi Theorem.

3. Dimensional Analysis using Buckingham-Pi Theorem

In an attempt to capture the dynamics of combined flow and heat-transfer experiments, relevant dimensionless parameters must be determined. An analysis of relevant dimensionless parameters for the non-rotating and rotating cases was conducted. Relevant parameters in the problem were determined and are summarized in Table 1 below.

TABLE 1. Relevant parameters for non-rotating and rotating flow through cylindrical pipe

Parameter	Description	Unit
v	Mean axial velocity	m/s
D	Diameter of pipe	m
ϑ	Kinematic viscosity	m^2/s
ρ	Density	kg/m^3
L	Axial length	m
Ω_o	Rotation rate of channel	$1/s$
k	Thermal conductivity	$W/(mK)$
α	Thermal diffusivity	m^2/s
ΔT	Temperature difference	K
h	Coefficient of convective heat transfer	$W/(m^2K)$

In conducting an analysis of the relevant dimensionless parameters for each problem, we can apply the Buckingham Pi-Theorem. The Buckingham Pi-Theorem states that for n physical variables defining a problem and j independent fundamental physical quantities there are s relevant dimensionless parameters related by the equation,

$$s = n - j \tag{18}$$

3a. Non-Rotating Circular Pipe

For the non-rotating case, with an entry length (both thermal/hydrodynamic or only thermal/fully developed hydrodynamic), the independent physical variables characterizing the problem include v, D,ρ, α, ϑ, L, k, h, and ΔT. In the stationary case, the four relevant dimensionless numbers are typically listed as:

$$Re = \frac{vD}{\vartheta}, \qquad Pr = \frac{\vartheta}{\alpha}, \qquad L_e = \frac{L}{D}, \qquad Nu = \frac{hD}{k}$$

The two new dimensionless parameters introduced are the entrance length and the Nusselt number. As the flow enters the channel, there is an entrance length in which the thermal and hydrodynamic boundary layers develop. Nusselt number correlations will be derived for both the developing and fully-developed conditions for both the rotating and non-rotating cases. In addition, the Nusselt number appears. The Nusselt number is a dimensionless number which is a ratio of the convective to conductive heat transfer at a surface within the fluid. Larger Nusselt numbers correspond to higher convection heat transfer and are therefore more desirable in cooling applications.

3b. Rotating Circular Pipe

With channel rotation, the relevant dimensionless parameters include the entire set included in Table 1: v, D,ρ, α, ϑ, L, k, h, ΔT, and Ω_0. An extra pi-group from the non-rotating case appears, so that in the rotating case, there are five dimensionless groups.

$$Re = \frac{vD}{\vartheta}, \qquad Pr = \frac{\vartheta}{\alpha}, \qquad L_e = \frac{L}{D}, \qquad Nu = \frac{hD}{k}, \qquad Ro = \frac{\mathrm{v}}{2\mathrm{D}\Omega_0}$$

The Rossby number is a ratio of inertial to Coriolis forces in a rotating flow. The Rossby numbers we will deal with are small, meaning Coriolis forces will dominate over inertial forces.

4. Model Validation

The first cases to be considered are for stationary circular tubes with constant wall temperature for both hydrodynamically fully developed/thermally-developing flow and co-developing flow. The conditions are realized in computational fluid dynamics software, ANSYS FLUENT, and results are obtained and compared against correlations found in literature.

The model then considers the effects of rotation on internal flow within circular tubes. Ito [4] provides an empirical friction factor correlation for fully-developed flow in straight pipes of circular cross section rotating about an axis perpendicular to the flow direction. Simulations

are run in ANSYS FLUENT and the results compared to Ito's empirical results. After the flow model is validated, the Nusselt numbers for developing and fully developed flow are obtained.

In order to properly execute the model and obtain accurate results, grid independence must be achieved so that the results of the simulations are not a function of the quality of mesh used. Different meshes were used until the results were independent of the size of mesh used. A mesh with inflation around the cylinder walls was used.

4a. Forced Convection for Laminar Flow inside a Circular Tube under Constant Wall Condition

In a circular tube characterized by laminar, fully developed flow with constant surface temperature, the Nusselt number is a constant, independent of Re, Pr, and axial location.

$$\mathrm{Nu_D} = 3.66 \ for \ T_s = constant \tag{19}$$

However, for the entry region both temperature and velocity depend on axial position z and radial position r. In this case, the Nusselt number is a function of Re, Pr, and axial location. Convection heat transfer with laminar flow in a circular tube (Re<2300) was examined for developing and fully developed flow with constant temperature walls.

For fully developed flow in a pipe where $L \gg L_e$ with constant temperature walls, Nu=3.66. For laminar flow, the hydrodynamic entrance length can be estimated by [5]

$$\frac{L_e}{D} = 0.06Re \tag{20}$$

Two different correlations for laminar flow in the entry region were examined- one for fully-developed hydrodynamic, developing thermal flow and the second for co-developing (both thermally and hydrodynamically) flow. The Nusselt numbers are infinite at z=0 and decay asymptotically to the fully developed value ($Nu_D = 3.66$ in the case of constant temperature walls) as axial distance increases. Both entry length conditions were simulated in FLUENT. For entry length correlations, the Graetz number is created (allowed by the Buckingham Pi Theorem), which is a function of the three dimensionless parameters found above, Re, Pr, L_e, and where we instead use the variable z to denote axial location within the tube.

$$Gz_D = \left(\frac{D}{z}\right) RePr \tag{21}$$

The first correlation looked at is the simpler case of the two. This correlation is for a thermal entry length and is based on the assumption that thermal conditions develop in the presence of a fully developed velocity profile. This situation can be realized physically by an unheated starting length which precedes the portion where heat transfer occurs, or by specifying a laminar velocity profile at the inlet. The Hausen [3] correlation for average Nusselt number

with constant surface temperature with hydrodynamically developed, thermally developing flow is given by:

$$\overline{Nu}_D = 3.66 + \frac{0.0668 Gr_D}{1+0.04 Gr_D{}^{2/3}} \tag{22}$$

where $\overline{Nu}_D \equiv \frac{\bar{h}D}{k}$. To find the average convection coefficient, $\bar{h}$, Equation (23) is used

$$\bar{h} = \frac{Q_{conv}}{A_s \Delta T_{lm}} \tag{23}$$

where ΔT_{lm} is defined as

$$\Delta T_{lm} \equiv \frac{\Delta T_o - \Delta T_i}{\ln (\Delta T_o / \Delta T_i)} \tag{24}$$

Whatever heat is transferred to the fluid through convection goes into heating up the fluid, so that

$$Q_{conv} = \dot{m} c_p (\Delta T_o - \Delta T_i) \tag{25}$$

where

$$\dot{m} = \rho \bar{V} \frac{\pi}{4} D^2 \tag{26}$$

Substituting Equations (24), (25), and (26) above, we obtain

$$\overline{Nu}_D = \frac{\rho \bar{V} D^2 c_p}{4Lk} \ln \left(\frac{\Delta T_i}{\Delta T_o} \right) \tag{27}$$

CFD simulations were done to calculate the average Nusselt number for the thermal entry length, and Figure 2 shows the predicted Nusselt Number correlation and the results obtained from CFD.

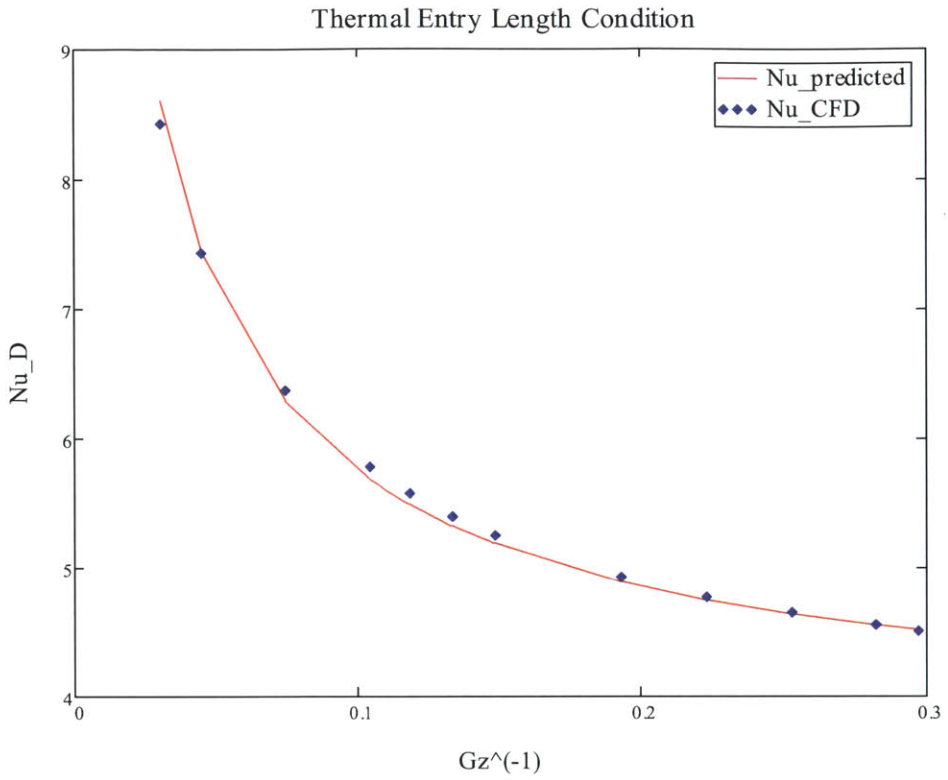

Figure 2. Average Nusselt number results obtained from thermal entry length correlation for laminar flow in a circular tube

In the second case, a combined (thermal and hydrodynamic) entry length is considered in which the temperature and velocity profiles develop simultaneously. For the combined entry length, the suitable correlation given by Sieder and Tate [2] is given in Equation (28).

$$Nu = 1.86(Gz)^{\frac{1}{3}}\left(\frac{\mu}{\mu_s}\right)^{0.14} \tag{28}$$

Sieder and Tate give the correlation for values of Prandtl number $0.48 < Pr < 16{,}700$ and for $0.0044 < \left(\frac{\mu}{\mu_s}\right) < 9.75$. The Sieder-Tate correlation also takes into account the change in viscosity (μ and μ_s). Since we have assumed constant properties, the $\frac{\mu}{\mu_s}$ term equals one in our case. The correlation has been recommended by Whitaker [7] for values of $Gz^{\frac{1}{3}}(\frac{\mu}{\mu_s})^{0.14} \geq 2$, which is met for all axial locations studied for this case.

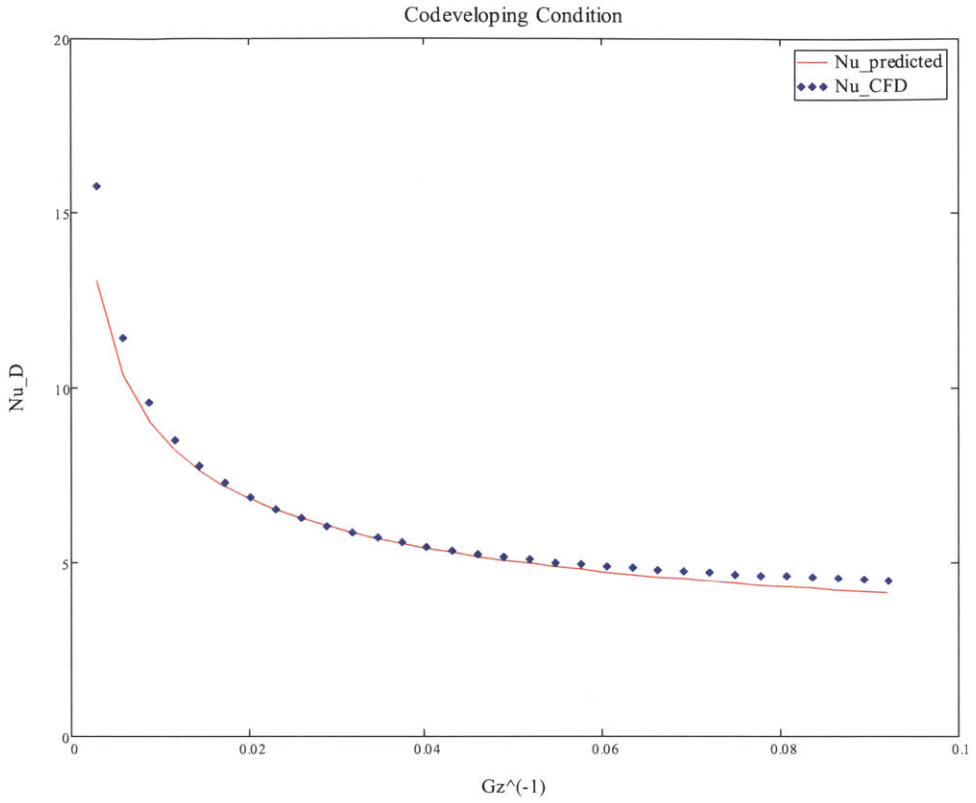

Figure 3. Average Nusselt number results obtained for laminar, combined entry length in a circular tube

As observed in Figures 2 and 3, the CFD model accurately predicts the Nusselt number as a function of Graetz number in the case of no rotation.

5. Cylindrical Tube Rotating Around Orthogonal Axis

5a. Friction Factor-Rotating Reference Frame

The pressure drop needed to sustain internal flow is of interest in engineering applications because it determines the pump or fan power requirements. The Moody or Darcy friction factor is a dimensionless parameter defined as

$$f \equiv -\frac{(dP/dx)D}{\rho v^2/2} \tag{29}$$

In order to derive the friction factor in the fully developed, laminar, rotating reference frame, the lumped hydrostatic pressure term P^* is used

$$\Delta P^* = P - \frac{1}{2}\rho\Omega^2 r^2 \tag{30}$$

where

$$r^2 = x^2 + z^2 \tag{31}$$

The friction factor for the fully-developed, laminar, rotating case can be found by

$$f = \frac{2\Delta P^* D}{L\rho v^2} \tag{32}$$

In the fully developed, laminar, rotating case, the friction factor is constant. The term ΔP^* can be found at two points within the fully developed regime by $\Delta P^* = \Delta P_o^* - \Delta P_i^*$. The friction factor is then found from the above equation.

In the case of fully developed laminar flow with no rotation, the friction factor is given by

$$f_{l,nr} = \frac{64}{Re} \tag{33}$$

Ito [4] gives an experimentally-derived friction factor equation for the fully developed, laminar, rotating friction factor as

$$\frac{f}{f_{l,nr}} = \frac{0.0883K_t^{\frac{1}{4}}}{\left[1-1.969K_t^{-\frac{1}{5}}\left(\frac{f}{f_{l,nr}}\right)^{-\frac{1}{5}}\right]^{\frac{5}{4}}} \tag{34}$$

where

$$K_t = ReR_\Omega \tag{35}$$

and R_Ω is a dimensionless parameter known as the rotational Reynolds number defined as

$$Ro = \frac{\Omega_0 D^2}{\vartheta} \tag{36}$$

The equation was said to give good agreement with experimental results in the range $K_t > 2 \times 10^3$ and $R_\Omega/Re < 0.5$ (Ito).

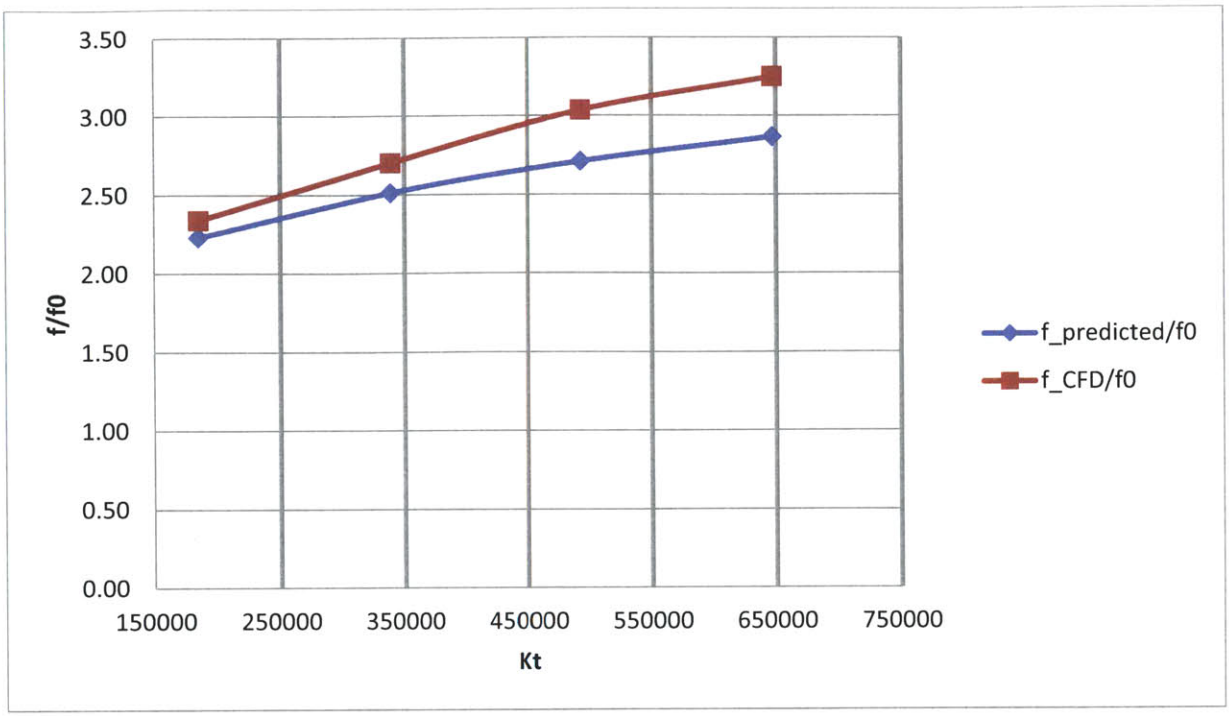

Figure 4. Friction factor results obtained for rotating laminar, fully-developed flow in cylindrical tube for Re~1,200

Our data falls within the ranges recommended by Ito for the correlation to be accurate. As observed in Figures 4, the CFD model accurately predicts the friction factor as a function of the rotational speed.

5b. Nusselt Number-Rotating Reference Frame

The axial and circumferential distribution of mean temperature is found for the constant surface temperature condition by the equation.

$$\frac{d(T_s - T_m)}{dzd\theta} = \frac{\pi Dh}{\dot{m}c_p}(T_s - T_m) \tag{37}$$

In the rotating case, the heat transfer coefficient will now be axially and circumferentially dependent. Integrating Equation (37), we obtain

$$\ln\left(\frac{\Delta T_o}{\Delta T_i}\right) = \frac{\pi DL}{2\dot{m}c_p}\int_0^L \int_0^{2\pi} h dz d\theta \tag{38}$$

The average heat transfer coefficient is thus

$$\bar{h} = \int_0^L \int_0^{2\pi} \frac{h}{2\pi L} dx d\theta \tag{39}$$

CFD simulations were run and corresponding Nusselt numbers for Re~1,200 and Re~2,000 as well as Rossby numbers, Ro~ 4.1, 2.2, 1.5, 1.7 were obtained. Plots of velocity profiles at the

outlet for no rotation, slow rotation, and fast rotation for the case Re~1,200 as well as contours of velocity for these cases are shown in the Results section.

6. Results

In the stationary fully developed laminar case, we observe the expected parabolic velocity profile. In the contour plot in Figure 5b, the core velocity at the center of the circular tube is highest and the flow is slowed down near the walls and zero at the walls by the no-slip condition.

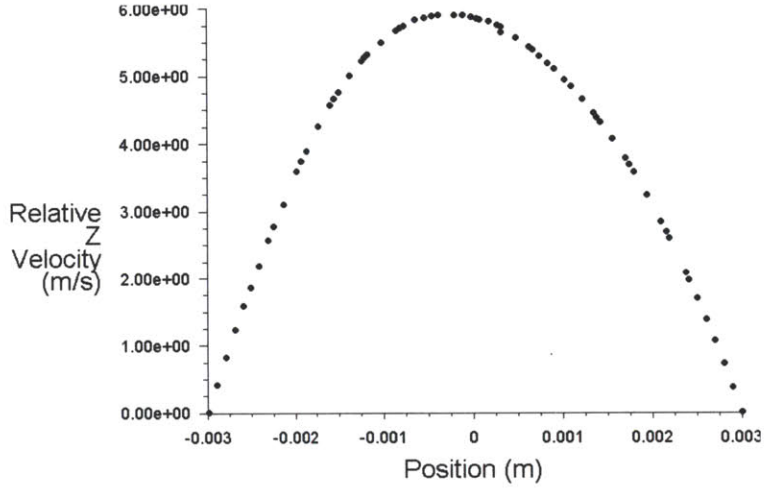

Figure 5a. Cross-section at outlet of circular tube showing parabolic velocity profile in stationary (i.e. no rotation) case

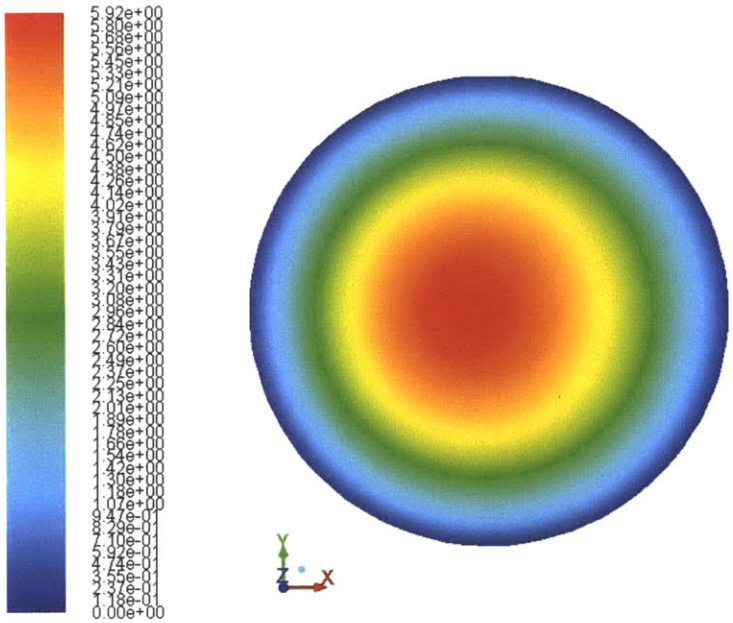

Figure 5b. Contours of z-velocity showing velocity distribution inside circular tube in non-rotating case

In Figure 6a with low rotation, instead of displaying the parabolic profile we expect in the stationary laminar case, the flow profile is shifted towards the trailing edge of the tube, away from the leading edge, resulting in an asymmetrical parabolic profile.

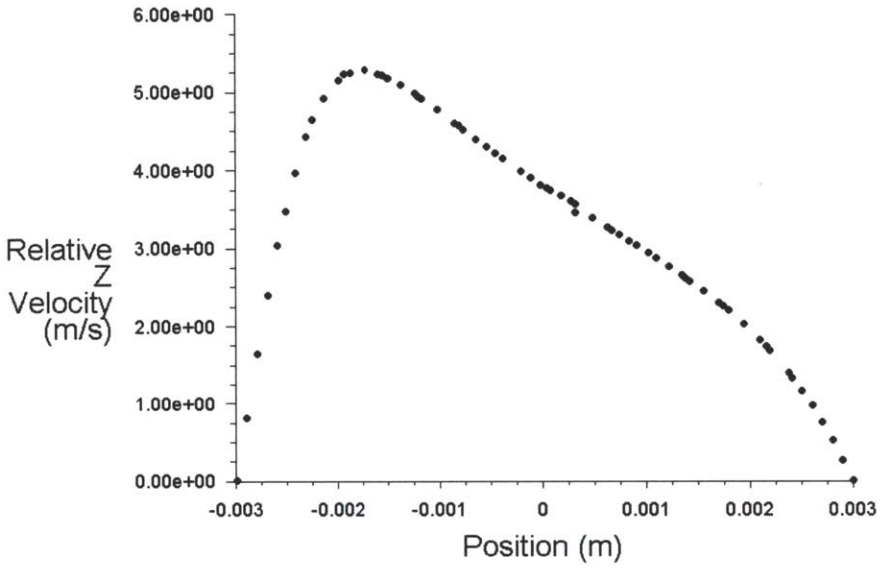

Figure 6a. Cross-section at outlet of circular tube showing parabolic velocity profile shift for low rotational speed, Ω_0= 60 rpm, for channel rotating counter-clockwise about the y-axis

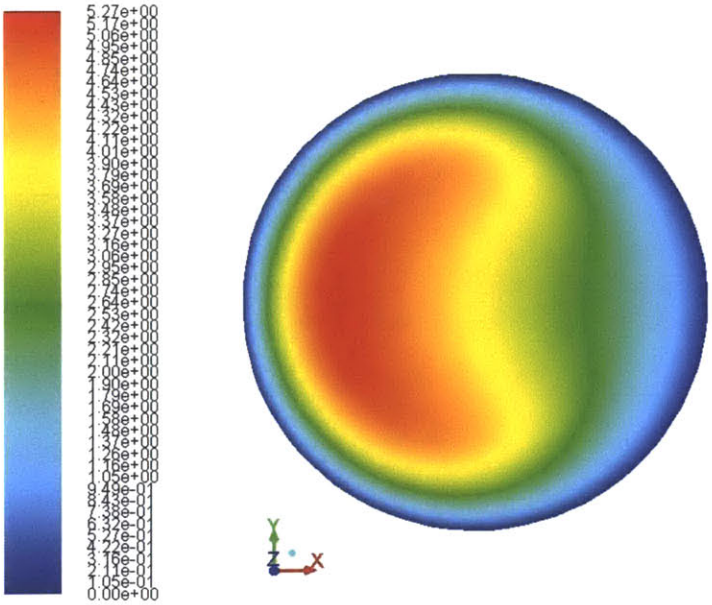

Figure 6b. Contours of z-velocity showing velocity distribution inside circular tube in low-rotation case for channel rotating counter-clockwise about the y-axis. Flow is shifted against trailing edge.

At higher rotational speeds, more of the flow is shifted towards the trailing edge of the tube. As seen in Figure 7b, this causes more of the flow to be slowed down as there is less of a presence of higher velocity in the contour plot.

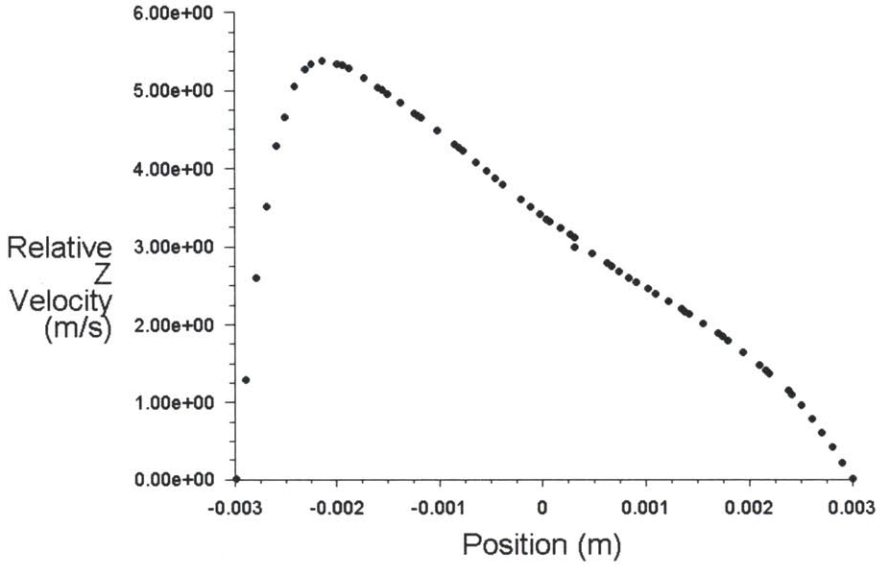

Figure 7a. Cross-section at outlet of circular tube showing parabolic velocity profile shift for rotational speed Ω_0= 300 rpm for channel rotating counter-clockwise about the y-axis

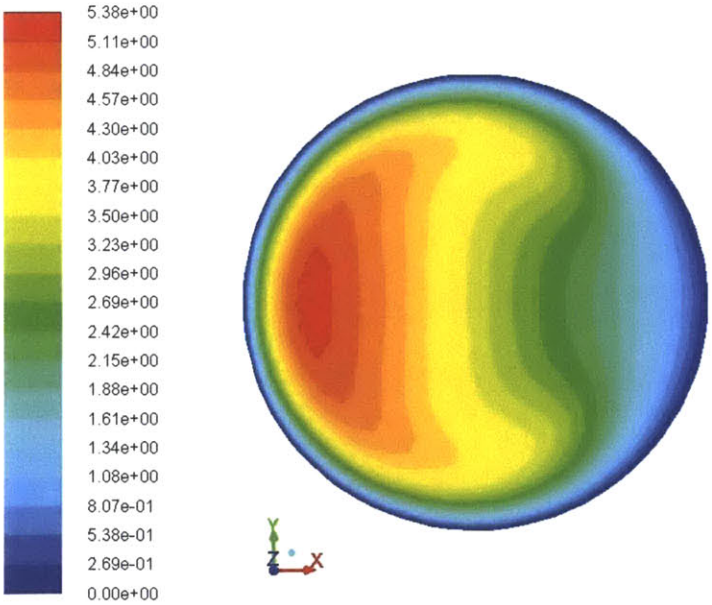

Figure 7b. Contours of z-velocity showing velocity distribution inside circular tube in rotation case Ω_0= 300 rpm for channel rotating counter-clockwise about the y-axis. Flow is shifted against trailing edge.

At the high rotation rate, we see the most shift toward the trailing edge of the wall with the maximum of the velocity profile the furthest shift to the left of all the cases. In addition, from the contour plot, the flow is slowed significantly from the low-rotation case.

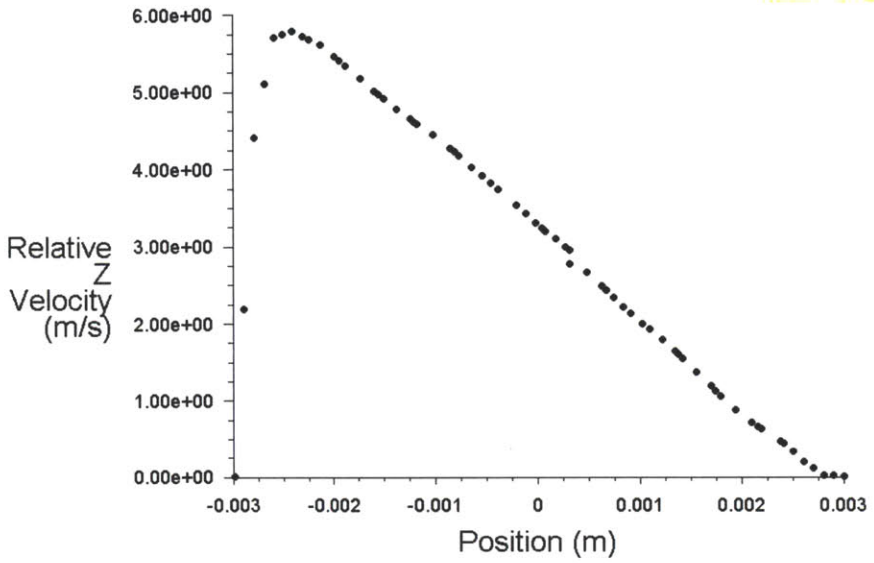

Figure 8a. Cross-section at outlet of circular tube showing parabolic velocity profile shift for high rotational speed, Ω_0= 2000 rpm, for channel rotating counter-clockwise about the y-axis

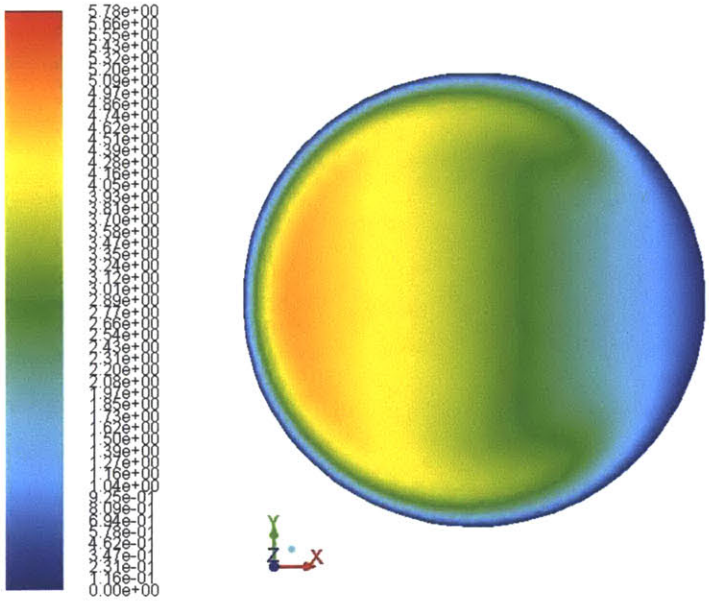

Figure 8b. Contours of z-velocity showing velocity distribution inside circular tube in rotation case Ω_0= 2000 rpm for channel rotating counter-clockwise about the y-axis. Flow is shifted against trailing edge.

In the high rotation case, the secondary flow caused by the Coriolis forces arising in the rotating reference frame is the greatest of the three cases. Secondary flows caused by Coriolis forces are said to increase heat-transfer effects. The following analysis presents and discusses data simulated for Re~1,200 and 2,000 and Ro~4.1, 2.2, 1.5, 1.7.

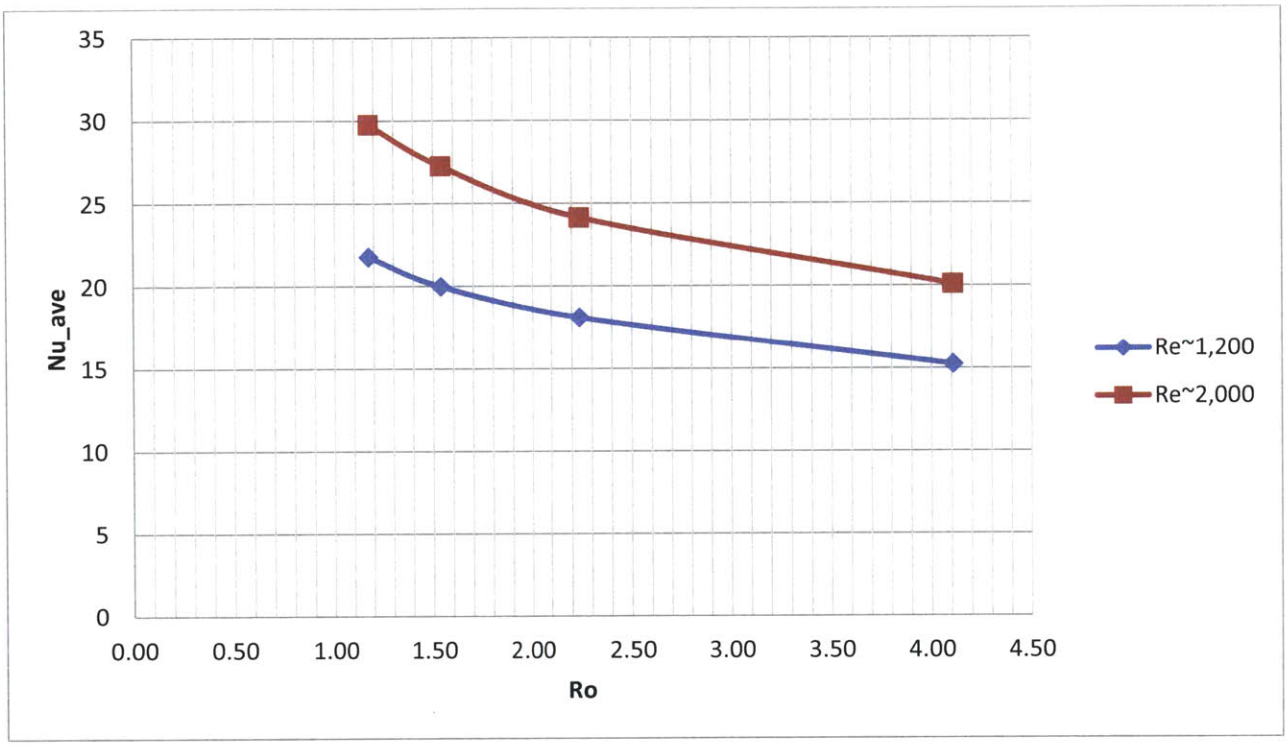

Figure 9. Average Nusselt number results obtained over length of tube for Ro~ 4.1, 2.2, 1.5, 1.7 and Re~1,200, 2,000. Increased heat transfer effect with increased rotation can be seen.

The average Nusselt number is higher at a given Rossby number for higher Reynolds number. Increasing rotational speed for a given Reynolds number leads to enhanced heat transfer effects. In the range of 1.2<Ro<4.1 for both Re~1,000, 2,000, the average Nusselt number increases about 50%.

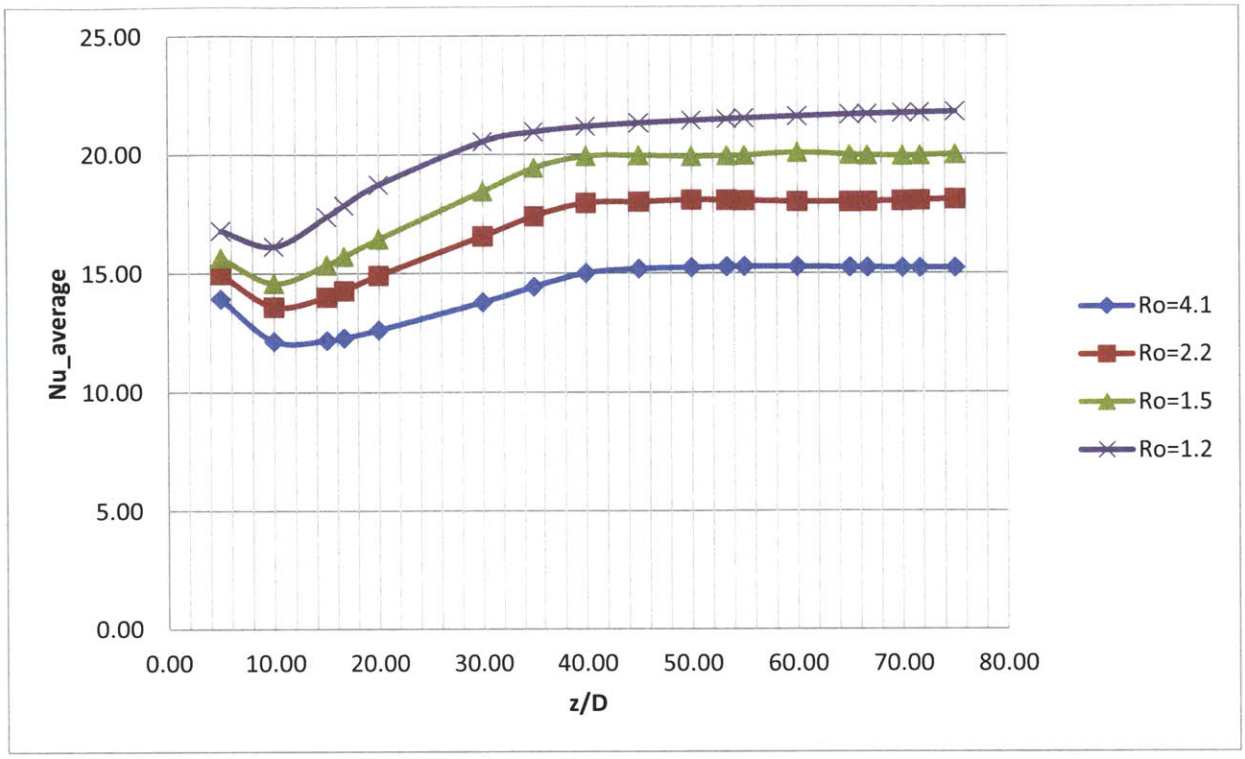

Figure 10. Average Nusselt number obtained for axial positions for Re~1,200 and Ro~4.1, 2.2, 1.5, 1.7. Increased heat transfer with increased rotation speeds can be seen.

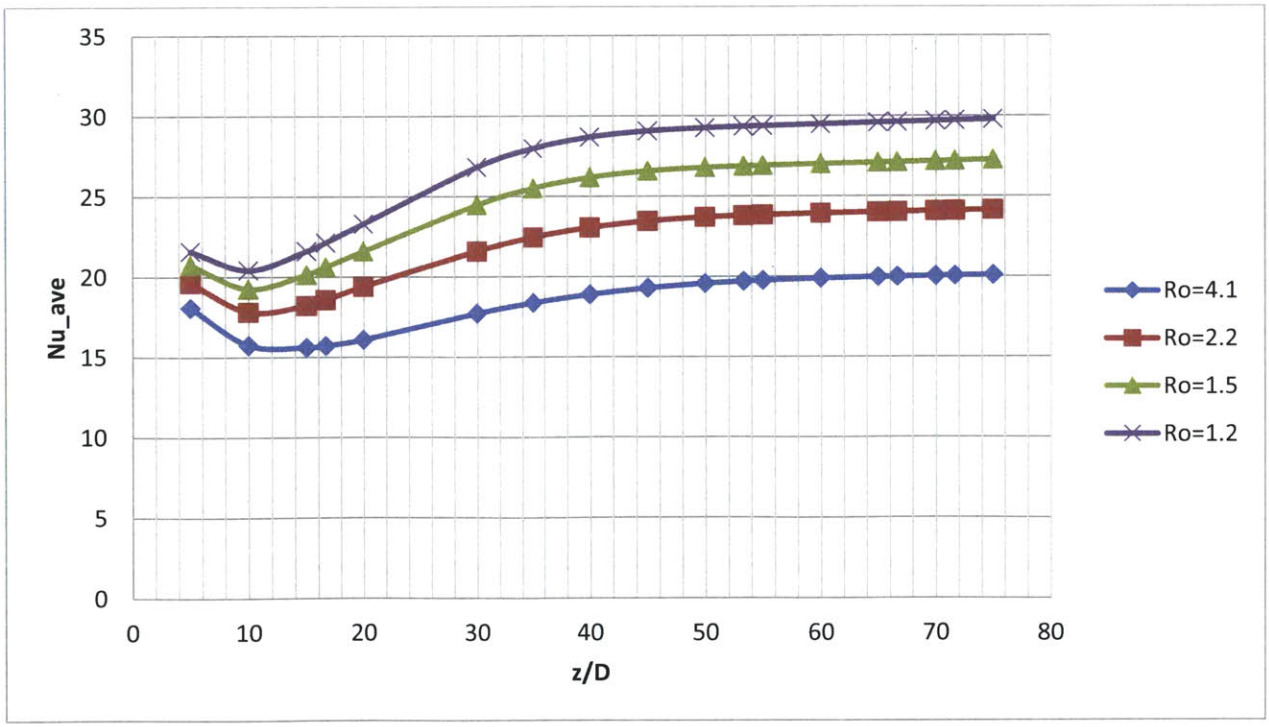

Figure 11. Average Nusselt number obtained for axial positions for Re~2,000 and Ro~4.1, 2.2, 1.5, 1.7. Increased heat transfer with increased rotation speeds can be seen.

In Figures 10 and 11, the average Nusselt number obtained for axial locations throughout the tube for a given Reynold's number and Rossby number are reported. Increased rotational speeds (decreased Rossby number) lead to increased heat transfer effects. Between the graphs, it can also be observed that increased Reynold's number for a given Rossby number results in increased heat transfer effects.

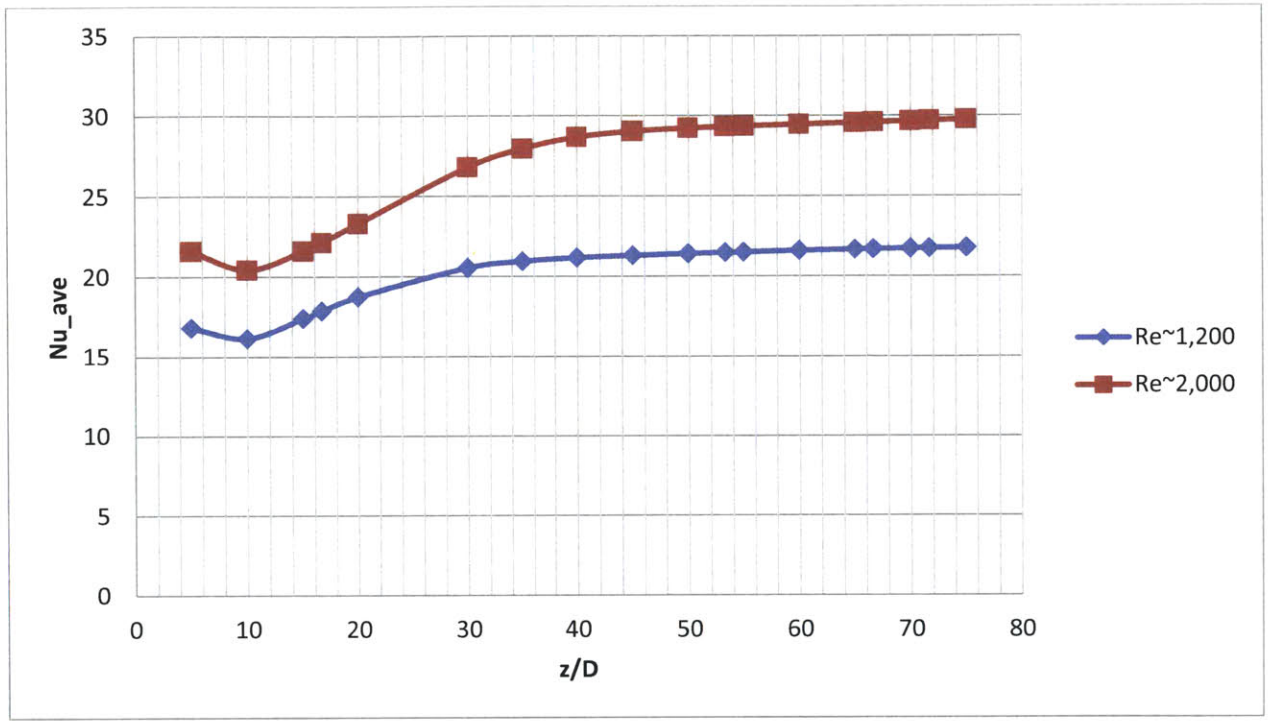

Figure 12. Average Nusselt number obtained for Ro~1.2 for Re~1,200 and Re~2,000. Enhanced heat transfer at given Rossby number for a larger Reynolds number.

Figure 12 shows the average Nusselt number obtained for Ro~1.2 and Re~1,200, 2,000. Enhanced heat transfer over the length of the tube is seen for a larger Reynolds number. Interestingly, the curves show a dip followed by an increase and plateau to a value at infinity. As seen in the stationary, constant wall temperature case, the coefficient of convective heat transfer is large in the entrance region and then decreases to a constant value in the fully developed region. In the rotating case, the Nusselt number first decreases, then increases, and finally plateaus to a higher value at infinity. The Coriolis forces due to rotation are interfering with the boundary layer development downstream so that increased heat transfer effects are seen downstream.

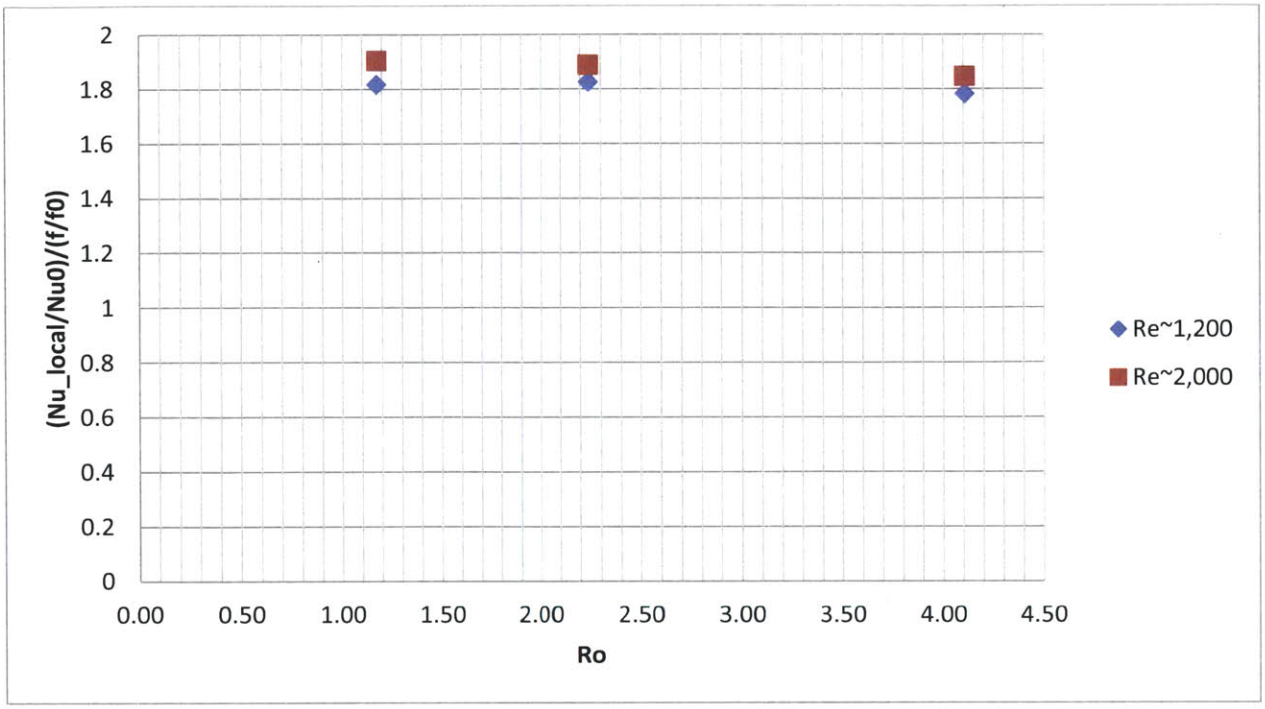

Figure 13. Ratio of heat transfer enhancement to friction losses

Figure 13 shows the ratio of heat transfer enhancement to friction losses as a function of the Rossby number which is of particular importance in cooling applications because it quantifies the price which must be paid for heat transfer enhancement (i.e. increased friction losses) with increased rotation. The data shows the ratio of heat transfer enhancement to friction factor penalty is always greater than one for every rotational speed, meaning that at any rotational speed, the heat transfer enhancement wins out over increased pressure drop. The ratio appears to remain fairly constant over the span of rotational numbers. This observation is consistent with the results seen in Figure 14, showing the ratio of heat transfer enhancement to friction factor as a function of Ro for the theoretical model. The theoretical model uses Mori and Fukata's [8] Nusselt number correlation and Ito's [4] friction factor correlation for $6.2<Ro<1.0$ and Re~1,200. Over the span of Rossby numbers from for $6.2<Ro<1.0$, the ratio shows about a 3% increase in value.

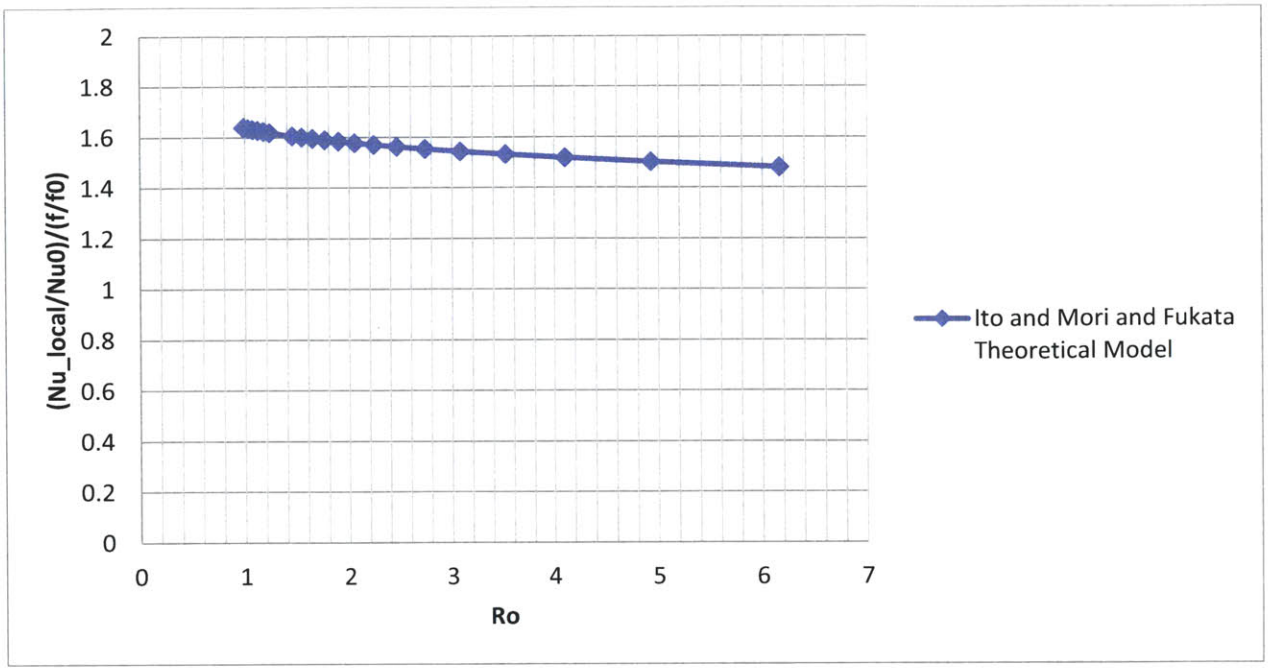

Figure 14. Ratio of heat transfer enhancement to friction factor as a function of Ro for theoretical model developed using Ito's [4] friction factor correlation and Mori and Fukata's [8] Nusselt number correlation for 6.2<Ro<1.0 and Re~1,200

7. Conclusion

Increasing rotation speed leads to increased heat transfer effects due to secondary flow caused by Coriolis forces. Rotation improves heat transfer from the stationary case by increasing heat transfer on the trailing edge of the channel compared to the leading edge, resulting in an overall increase in the convective heat transfer coefficient as well as an increase in the flow resistance from the stationary case. However, the data shows the ratio of heat transfer enhancement to friction factor penalty is always greater than one for every rotational speed, meaning that at any rotational speed, the heat transfer enhancement outweighs the increased pressure drop.

8. Bibliography

[1] B. M. Boubnov and G. S. Golitsyn (1995). Convection in Rotating Fluids. Springer, pp 5-10. ISBN 0-7923-3371-3.

[2] E. N. Sieder and G. E. Tate. *Ind. Eng. Chem.*, 28, 1429, 1936.

[3] H. Hausen. Z. VDI *Beih. Verfahrenstech.*, 4, 91, 1943.

[4] H. Ito and K. Nanbu (1970). "Flow in Rotating Straight Pipes of Circular Cross Section," ASME paper No. 70-WA/FE-13.

[5] Incropera et al (2002). Fundamentals of Heat and Mass Transfer. pp 465-490. ISBN 0-471-38650-2.

[6] W. D. Morris. "Rotating Facility to Study Heat Transfer in Cooling Passages of Turbine Rotor Blades," Proceedings of the Institution of Mechanical Engineers, Part A: Journal of Power and Energy 1996. online version: http://pia.sagepub.com/content/210/1/55.

[7] Whitaker, S., *AIChE J.*, 18, 361, 1972.

[8] Y. Mori and T. Fukada. "Convective Heat Transfer in Rotating Radial Circular Pipe (2^{nd} report)." *Int. J. Heat Mass Transfer*, 14, pp 1807-1824, 1971.